Hindawi Publishing Corporation
Journal of Fuels
Volume 2015, Article ID 915015, 9 pages
http://dx.doi.org/10.1155/2015/915015

Research Article

Petroleum Diesel and Biodiesel Fuels Used in a Direct Hydrocarbon Phosphoric Acid Fuel Cell

Yuanchen Zhu,[1,2] André Y. Tremblay,[1] Glenn A. Facey,[3] and Marten Ternan[1,2,4]

[1]*Chemical and Biological Engineering, University of Ottawa, 161 Louis Pasteur, Ottawa, ON, Canada K1N 6N5*
[2]*Catalysis Centre for Research and Innovation, University of Ottawa, 30 Marie Curie, Ottawa, ON, Canada K1N 6N5*
[3]*Chemistry, University of Ottawa, 10 Marie Curie, Ottawa, ON, Canada K1N 6N5*
[4]*EnPross Incorporated, 147 Banning Road, Ottawa, ON, Canada K2L 1C5*

Correspondence should be addressed to Marten Ternan; ternan@bell.net

Received 4 July 2015; Accepted 13 September 2015

Academic Editor: Zhongliang Zhan

The performance of a direct hydrocarbon phosphoric acid fuel cell, PAFC, was investigated using petroleum diesel, biodiesel, and n-hexadecane as the fuels. We believe this is the first study of a fuel cell being operated with petroleum diesel as the fuel at the anode. Degradation in fuel cell performance was observed prior to reaching steady state. The degradation was attributed to a carbonaceous material forming on the surface of the anode. Regardless of the initial degradation, a steady-state operation was achieved with each of the diesel fuels. After treating the anode with water the fuel cell performance recovered. However, the fuel cell performance degraded again prior to obtaining another steady-state operation. There were several observations that were consistent with the suggestion that the carbonaceous material formed from the diesel fuels might be a reaction intermediate necessary for steady-state operation. Finally, the experiments indicated that water in the phosphoric acid electrolyte could be used as the water required for the anodic reaction. The water formed at the cathode could provide the replacement water for the electrolyte, thereby eliminating the need to provide a water feed system for the fuel cell.

1. Introduction

The long-term objective of this research is to replace the diesel fuel combustion engines currently used in rail locomotives with fuel cell stacks operating on low sulphur (15 ppm) diesel fuel. Fuel cells have at least three advantages.

Greater energy efficiency is one advantage. The maximum operating temperature of the steel in combustion engines limits the engine's theoretical Carnot energy efficiency to about 67%. Many types of fuel cells operate at much lower temperatures and are not limited by the temperature characteristics of materials. Theoretically some fuel cells can have much greater energy efficiencies than combustion engines.

Diminished emissions of both greenhouse gas emissions (CO_2, CH_4, and N_2O) and other air contaminants (NO_X, CO, HC, SO_X, and particulate matter) are another advantage. Because fuel cells are expected to have greater energy efficiency they will use less fuel and therefore emit less CO_2 and less SO_X. The formation of N_2O and NO_X by reaction between O_2 and N_2 in air is thermodynamically unfavorable at low fuel cell operating temperatures (<200°C). CH_4 is not produced because H radicals from diesel fuel become protons and are not available to form CH_4. Oligomerized hydrocarbon molecules that might become particulate matter = PM are adsorbed by the fuel cell catalyst. Because CO is strongly adsorbed by platinum fuel cell catalysts, it is unlikely to be emitted.

Diminished locomotive idling is another advantage. Low temperature (<200°C) fuel cells can start and stop quickly. The rapid start-up ability would also permit locomotives to shut down on some of the occasions during which locomotive combustion engines must continue to operate at "idle" in accordance with the existing standard practice. That would use less fuel and both increase energy efficiency and diminish emissions.

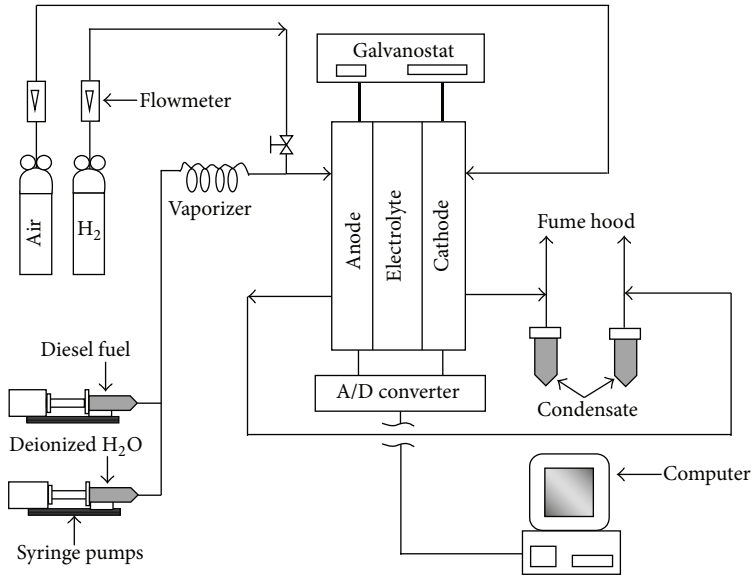

Figure 1: Diagram of a direct hydrocarbon phosphoric acid fuel cell system.

There is another advantage. Fuel cells have almost no moving parts. As a result maintenance costs for fuel cells may be a fraction of those for combustion engines.

In this work the performance of real diesel fuels (petroleum diesel and biodiesel) and n-hexadecane, a pure compound used as a model for diesel fuel (Cetane Number = 100), was investigated in a low temperature ($T < 200^{\circ}C$) phosphoric acid fuel cell. Currently fuel cells using hydrogen fuel are being used in locomotives for underground mining where constraints on air quality exist. However, technology for fuel cells using real diesel fuel in locomotives operating above ground is essentially nonexistent.

Real diesel fuels are composed of many different compounds. As a result many different reactions will occur in fuel cells that use them as fuels. The reactions with the n-hexadecane model compound provide a basis for an extrapolation to real diesel fuels that may indicate the complexity of their reactions.

In a direct n-hexadecane phosphoric acid fuel cell, the overall reaction is

$$C_{16}H_{34}\,(g) + \frac{49}{2}O_2\,(g) \longrightarrow 16CO_2\,(g) + 17H_2O\,(g) \quad (1)$$

The anode half-cell reaction is

$$C_{16}H_{34}\,(g) + 32H_2O\,(g) \longrightarrow 16CO_2\,(g) + 98H^+ + 98e^- \quad (2)$$

The cathode half-cell reaction is

$$\frac{49}{2}O_2\,(g) + 98H^+ + 98e^- \longrightarrow 49H_2O\,(g) \quad (3)$$

where the (g) represents the gas phase. The anode stoichiometric ratio, $SR = H_2O/C_{16}H_{34}$, is 32. One mole of n-hexadecane reacts with 32 moles of water at the anode and generates 98 moles of protons and electrons. The protons migrate through the electrolyte to the cathode where the oxygen reduction reaction occurs.

Very few studies of fuel cells operating with commercially available diesel fuels have been reported. Almost all of the reports available in the literature have been performed using high temperature (700–1000°C) solid oxide fuel cells. Zhou et al. [1] used jet fuel. Sasaki et al. [2, 3] performed two studies using biodiesel. Kim et al. [4] used a synthetic diesel fuel. The other studies were performed using pure compounds, n-hexadecane [5], dodecane [6], and isooctane [7]. The only study using a lower temperature (150°C) phosphoric acid fuel cell was performed with a series of pure n-alkane compounds from methane to n-hexadecane [8].

Direct hydrocarbon fuel cells, DHFCs, operating at low temperature were investigated in the past. The extensive research on direct hydrocarbon fuel cells that was performed in the 1960s has been documented in three reviews [9–11]. Since then research on DHFCs has continued. Low temperature fuel cell studies (<100°C) were performed on methane by Bertholet [12] and on propane by Cheng et al. [13] and by Savadogo and Rodríguez Varela [14, 15]. Heo et al. [16] performed intermediate temperature fuel cell studies (100–300°C) using propane.

Phosphoric acid fuel cell technology using hydrogen as a fuel is used in commercial practice. By the year 2006 more than 200 commercial plants had been sold [17]. Appleby [18] has described the current state of PAFC technology using hydrogen as a fuel.

2. Experimental

A schematic diagram of the direct diesel fueled phosphoric acid fuel cell system (PAFC) is shown in Figure 1. The overall system consists of an air cylinder, a hydrogen cylinder, one galvanostat, two syringe pumps, a vaporizer, a phosphoric acid fuel cell (PAFC = Electrochem FC-25-02MA), and a fuel cell test station. Both gaseous and liquid fuels can be used in this fuel cell system. Deionized water and a diesel fuel were

introduced into the vaporizer by separate syringe pumps. The liquid fuels were expected to vaporize before reaching the anode of the fuel cell. Air was fed to the cathode at a constant flow rate. On those occasions when hydrogen was used as the fuel, the pumps were stopped and the valve in Figure 1 was opened.

Three diesel fuels were compared with n-hexadecane. The petroleum diesel fuel was purchased from an Imperial Oil service station. It meets the specifications in the American Standards for Testing Materials standard ASTM D-975. Its minimum cetane number is 40 and its sulphur content was less than 15 ppm. The soybean biodiesel used in this study was produced from degummed soybean oil. The following reagents were used in its production: sodium methoxide (25 wt% in methanol solution, Sigma Aldrich), methanol (Assay: 99.3–99.9%, Optima grade, Fisher scientific), and hydrochloric acid (36.5–38%, reagent grade, Fisher scientific). The soybean biodiesel was produced by transesterifying degummed soybean oil in a two-stage process using a solution of sodium methoxide in methanol. The first transesterification was performed in a membrane reactor [19] using a mole ratio of 5/1 methanol to oil. The methanol used in this reaction contained 0.5 wt% sodium methoxide on an oil basis. The mixture having passed through the membrane was further reacted in a batch process using a mole ratio of 2/1 methanol to oil. The methanol in the second reaction contained 0.2 wt% sodium methoxide catalyst on an oil basis. The fatty acid methyl ester, FAME, from the second reaction was neutralized and washed with water and then dried under vacuum. It was tested and met ASTM 6751 and EN14105 standards for glycerol and mono-, di-, and triglycerides. The biodiesel produced from canola oil was purchased from Milligan Biofuels Inc. (Foam Lake, SK, Canada). It was used as received from the manufacturer and is referred to here as "canola-biodiesel." It was specified to have a cetane number of 50.34 and a sulphur content of 2.8 ppm.

The membrane electrode assembly (MEA) used in our fuel cell work had five layers: two gas diffusion layers (GDL), two catalyst layers (CL), and a liquid electrolyte layer. The gas diffusion layers were Teflon coated Toray paper. The liquid electrolyte was initially 85% (14.6 M) phosphoric acid, which was held in a SiC matrix between the anode and cathode catalyst layers. Platinum (0.5 mg Pt/cm^2) supported on carbon (10% Pt on C) was the catalyst in both anode and cathode catalyst layers. The fuel cells had a face area of 25 cm^2. A pin-type flow field was machined in a graphite plate. The current collectors were sheets of copper metal that had been gold plated on both sides. Silicone rubber flexible heaters were attached to each current collector.

Several types of experiments were performed. A polarization curve shows the potential difference as a function of current density. Diesel fuel polarization curves were measured. Three types of time-on-stream experiments were performed (H_2O with diesel fuel, n-$C_{16}H_{34}$ only, and H_2O only). The time-on-stream experiments were performed at (a) an anode diesel fuel flow rate of 0.2 mL/h, anode water flow rate of 5.1 mL/h, cathode air flow rate of 245 mL/min, (b) current densities of 0.4 mA/cm^2, and (c) a temperature of

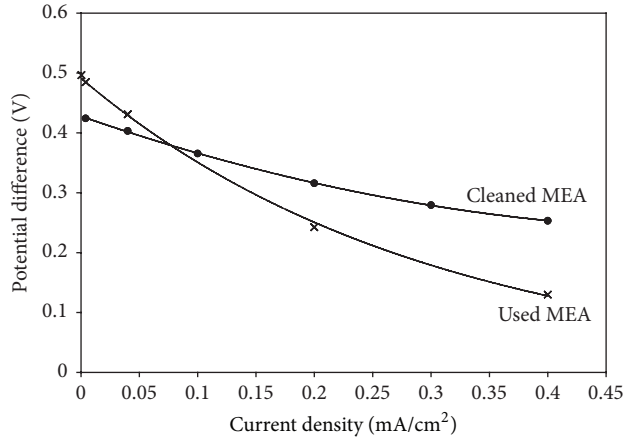

Figure 2: Polarization curve for an n-hexadecane fueled PAFC: potential difference between the electrodes (V) versus current density (mA/cm^2). Anode: water flow rate = 5.1 mL/h and n-hexadecane flow rate = 0.2 mL/h. Cathode: air flow rate = 245 mL/min. Temperature = 190°C. Pressure = 1 atm.

190°C and a pressure of 1 atm. Hydrogen polarization curves were measured to determine the state of the MEA in the fuel cell, using an anode hydrogen flow rate of 9.6 mL/min, cathode air flow rate of 245 mL/min, a temperature of 160°C, and a pressure of 1 atm.

A Hokuto Denko HA-301 Galvanostat was used to adjust the potential difference between the anode and cathode of the phosphoric acid fuel cell to maintain the chosen current at a constant value. The potential difference was recorded every second using a Lab View data logger.

Concentrated petroleum diesel or biodiesel samples were prepared in $CDCl_3$ and placed in 5 mm NMR tubes. The volume ratio of sample to $CDCl_3$ was approximately 80 : 20. All ^{1}H and ^{13}C NMR data were collected on a Bruker AVANCE 500 NMR spectrometer operating at 500.13 MHz and 125.77 MHz for ^{1}H and ^{13}C, respectively. The ^{1}H NMR spectra were collected using a 30° pulse, 16 scans, and a 3.9-second interpulse spacing. The time domain data were processed without apodization. The ^{13}C NMR spectra with inverse gated ^{1}H decoupling were collected using a 30° pulse, a 60-second recycle delay, and at least 1024 scans. Under these conditions the ^{13}C NMR spectra were deemed to be semiquantitative. ^{13}C DEPT-135 spectra were collected with a 2-second recycle delay and at least 32 scans. All ^{13}C time domain data were processed with 3 Hz of exponential line broadening.

3. Results and Discussion

Polarization curves for a phosphoric acid fuel cell operating on n-hexadecane are shown in Figure 2. As with all polarization curves, the potential difference decreases as the current density increases. The decrease is greater for the polarization curve obtained with the used MEA than with the cleaned MEA. As will be explained later, carbonaceous

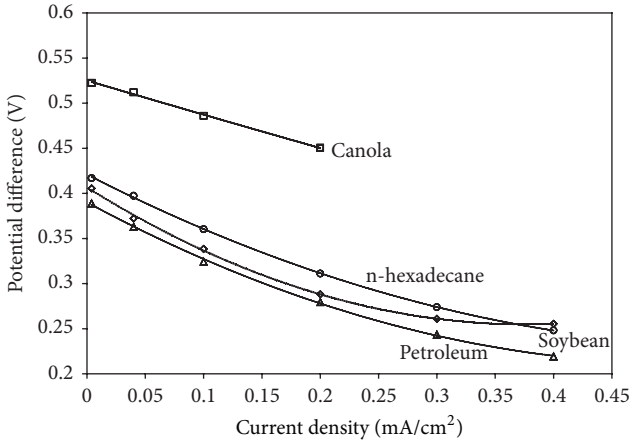

Figure 3: Potential difference between the electrodes (V) versus current density (mA/cm^2) for a diesel fuel/water PAFC. Anode: water flow rate = 5.1 mL/h and fuel flow rate = 0.2 mL/h. Cathode: air flow rate = 245 mL/min. Temperature = 190°C. Pressure = 1 atm.

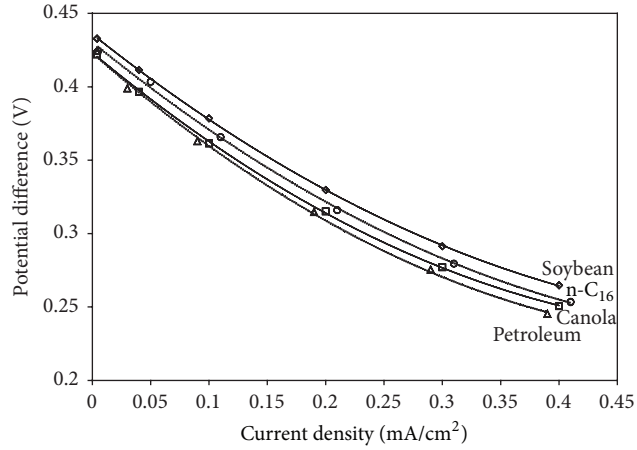

Figure 4: Potential difference between the electrodes (V) versus current density (mA/cm^2) for a diesel fuel/water PAFC. Current density j = 0.04 mA/cm^2. Anode: water flow rate = 5.1 mL/h and fuel flow rate = 0.2 mL/h. Cathode: air flow rate = 245 mL/min. Temperature = 190°C. Pressure = 1 atm.

deposits may have accumulated on the used MEA during previous experiments. The larger decrease in potential difference observed with the used MEA might have been caused by a greater quantity of carbonaceous material on the anode surface and therefore by the availability of a smaller number of catalyst sites. It should be noted that the potential difference at open circuit potential (at current density = zero) is somewhat greater for the used MEA than for the cleaned MEA. This phenomenon is also apparent in some of the other data in subsequent figures. One explanation is that the accumulated carbonaceous deposits on the used MEA provide more reactant than is available on the cleaned MEA.

Polarization curves for several diesel fuels, petroleum diesel, canola biodiesel, and soybean biodiesel are compared with n-hexadecane in Figure 3. Each of the data sets was obtained immediately prior to the beginning of a time-on-stream, TOS, experiment with the same diesel fuel. The data for the canola biodiesel were obtained using a recently cleaned MEA. The data for the other diesel fuels were obtained with an MEA that had been used for many experiments prior to the measurements in Figure 3. The data obtained with the used MEA are substantially worse than those obtained with the recently cleaned MEA. The diminished performance with the used MEA in Figure 3 is consistent with an accumulation of carbonaceous deposits during the prior TOS experiments. CO poisoning of the platinum catalyst would have been an alternative explanation for the degradation in fuel cell performance. That explanation was discounted since the rapid oscillations in potential difference [20] observed with CO poisoning were not observed here.

Polarization curves for the same four fuels, measured with a used MEA following each of their respective 15-hour TOS experiments, are shown in Figure 4. They are generally similar to one another. The open circuit potential after the TOS experiments, in Figure 4, is slightly greater for each fuel than that at the beginning of the TOS experiments in Figure 3. That observation is consistent with the data in Figure 2.

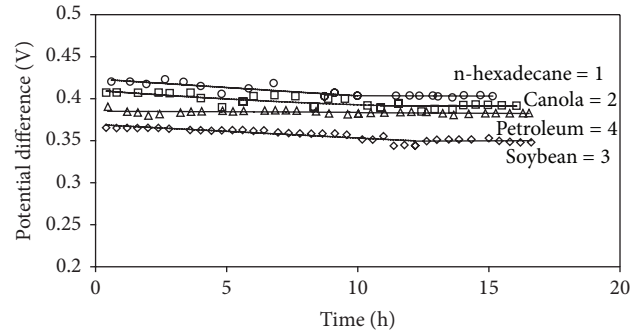

Figure 5: Potential difference between the electrodes (V) versus time-on-stream (h) for a diesel fuel/water PAFC. Current density j = 0.04 mA/cm^2. Anode: water flow rate = 5.1 mL/h and fuel flow rate = 0.2 mL/h. Cathode: air flow rate = 245 mL/min. Temperature = 190°C. Pressure = 1 atm.

Measurements of potential difference across the fuel cell using four different feedstocks, petroleum diesel, canola biodiesel, soybean biodiesel, and n-hexadecane are compared as a function of TOS in Figure 5. The numbers on the figures represent the sequence in which the experiments were performed. Initially a degradation in fuel cell performance occurred. However, for all feedstocks a steady-state operation was obtained during the last 6 hours of operation. For petroleum diesel a steady-state operation was observed throughout the 15-hour period. The steady-state operation was an indication that there was no additional degradation in fuel cell performance. That was interpreted as there being no additional net accumulation of carbonaceous material. However, the carbonaceous material hypothesized previously would have been present on the anode surface during the steady-state operating periods. That suggests that the carbonaceous material might have been a reaction intermediate. The rate of its reaction to form products would have been equal to its rate of formation if there was no net accumulation.

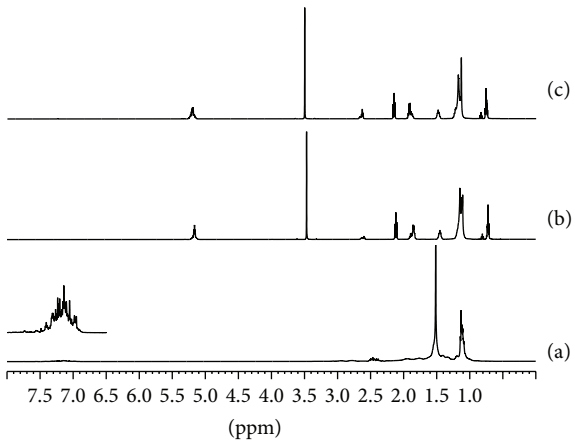

Figure 6: ^{1}H NMR spectra for (a) petroleum diesel (with vertically expanded inset showing the aromatic protons); (b) canola biodiesel; and (c) soybean biodiesel.

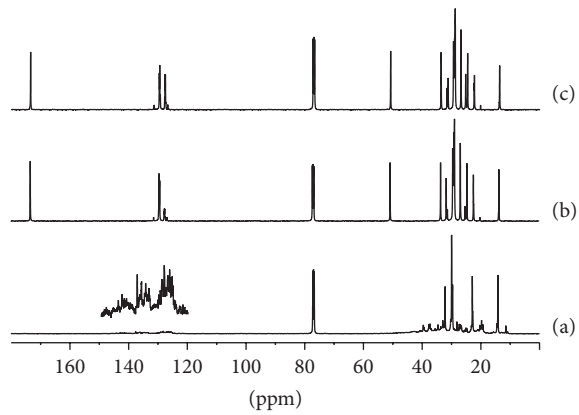

Figure 7: Quantitative ^{13}C NMR spectra for (a) petroleum diesel (with vertically expanded inset showing the aromatic carbons); (b) canola biodiesel; and (c) soybean biodiesel.

The formation of carbonaceous material in direct hydrocarbon fuel cells has been reported previously [11].

The diesel fuels in Figure 5 have different compositions which are conveniently analyzed via NMR spectroscopy. The ^{1}H NMR spectra of petroleum diesel, canola biodiesel, and soybean biodiesel are shown in Figure 6 (a), (b), and (c), respectively.

Petroleum diesel is a complex mixture of primarily aliphatic hydrocarbons. However, there is a small aromatic component shown in the vertically expanded inset of Figure 6(a). The aromatic protons are in the 6.5 ppm–8 ppm range. The aliphatic CH, CH_2, and CH_3 protons are in the 4 ppm–0 ppm range. The ratio of aromatic/aliphatic protons is 1/35.7. Canola and soybean biodiesel consist of the methyl esters of the fatty acids derived from the corresponding triglyceride oils. The ^{1}H NMR spectra of the two biodiesel samples are similar in general appearance. Unlike petroleum diesel, there are no aromatic protons in the canola or soybean biodiesels. There are, however, olefinic CH protons at ~5 ppm. The CH_2 protons are between 1 ppm and 3 ppm. The CH_3 protons terminating the aliphatic chains are between 0.5 ppm and 1 ppm. The large peak at ~3.5 ppm represents the $-OCH_3$ methyl groups of the methyl esters. The major difference between the ^{1}H NMR spectra of the biodiesels is in the group of resonances at 2.63 ppm which represents CH_2 protons between C=C double bonds (–C=C–CH_2–C=C–). The soybean biodiesel has more intensity in this region compared to canola biodiesel, consistent with the fact that soybean oil contains more polyunsaturated fatty acids than canola oil [21].

The quantitative ^{13}C NMR spectra of petroleum diesel, canola biodiesel, and soybean biodiesel are shown in Figure 7 (a), (b), and (c), respectively.

The spectrum of petroleum diesel in Figure 7(a) reflects the predominantly aliphatic nature of the petroleum diesel. The aliphatic CH, CH_2, and CH_3 ^{13}C resonances are between 10 ppm and 50 ppm. The vertically expanded inset shows more clearly the aromatic carbons in the petroleum diesel in the range 120 ppm–150 ppm. A ^{13}C DEPT-135 spectrum of the petroleum diesel showed that the ^{13}C resonances between 132 ppm and 150 ppm are due only to quaternary aromatic carbon atoms whereas the resonances between 120 ppm and 132 ppm are due to aromatic CH carbon atoms. The DEPT 135 data also revealed that there were no detectable quaternary aliphatic carbon atoms. The ^{13}C NMR spectra of the biodiesels are similar in general appearance. In these spectra the olefinic CH resonances are between 126 ppm and 132 ppm. The CH_2 resonances are between 20 ppm and 35 ppm. The CH_3 groups terminating the fatty acid chains are at ~14 ppm. The OCH_3 and carbonyl carbons of the methyl esters are at ~51 ppm and ~173 ppm, respectively. The composition data obtained from the ^{1}H and ^{13}C NMR spectra are summarized in Table 1 compared to the composition data for n-hexadecane obtained by its structural formula.

The resistance to current, $E^0 - \Delta\Phi$, can be related to the sum of the overpotentials at the anode and cathode plus the ohmic polarization. E^0 is the standard electrochemical potential (e.g., $E^0 = 1.09$ V for hexadecane/oxygen). $\Delta\Phi$ is the measured potential difference between the anode and the cathode. For the various feedstocks, the fuel cell potential differences were ordered from largest to smallest as follows: n-hexadecane, canola biodiesel, petroleum diesel, and soybean biodiesel. This trend correlates with both the H/C ratio and the total % CH_2 of the feedstock. It implies that the resistance to current in the fuel cell may be related to the number of available aliphatic hydrogen atoms per carbon atom in the feedstock. The feedstock with the largest H/C ratio had the smallest resistance to current. There does not appear to be an obvious relationship between the potential difference across the fuel cell and the percentage of olefinic or aromatic CH protons in the feedstock.

Additional experiments with n-hexadecane are seen in Figure 8 as potential difference versus time-on-stream. The first experiment in the sequence, n-hexadecane from Figure 5, is compared with the fifth experiment, also with n-hexadecane. For the fifth experiment, a steady-state operation was observed throughout the 15-hour period. Therefore,

Table 1: Carbon types in diesel fuels.

	n-hexadecane	Petroleum diesel	Canola biodiesel	Soybean biodiesel
CH (olefinic)	0%	—	6.8%	8.5%
CH (aromatic)	0%	2.7%	0%	0%
CH_2 (total)	82.4%	>70%	76.3%	74.1%
CH–$\mathbf{CH_2}$–CH	0%	—	1.7%	3.8%
–(CO)–$\mathbf{CH_2}$	0%	—	5.7%	5.8%
–(CO)–CH_2–$\mathbf{CH_2}$–	0%	—	5.9%	5.9%
–CH_2–$\mathbf{CH_2}$–CH=CH	0%	—	10.4%	9.5%
–$(CH_2)_n$–	82.4%	—	52.6%	49.1%
C–$\mathbf{CH_3}$	17.6%	—	8.7%	8.8%
O–$\mathbf{CH_3}$	0%	—	8.2%	8.6%
H : C ratio	2.125	1.84	1.85	1.83

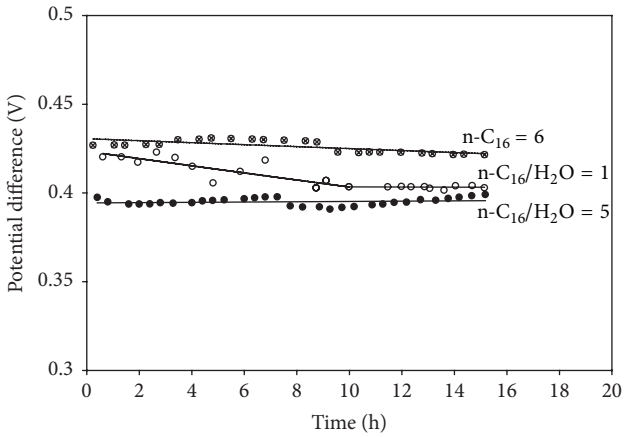

Figure 8: Potential difference between the electrodes (V) versus time-on-stream (h) for an n-hexadecane PAFC. Current density $j = 0.04$ mA/cm^2. For the first and fifth experiment the values of the variables were as follows. Anode: water flow rate = 5.1 mL/h and n-hexadecane flow rate = 0.2 mL/h. Cathode: air flow rate = 245 mL/min. Temperature = 190°C. Pressure = 1 atm. For the sixth experiment, there was no water flow.

based on these data in Figures 5 and 8, it can be stated with some confidence that it is possible to operate a direct hydrocarbon fuel cell with a variety of diesel fuels at steady state for at least several hours.

The sixth experiment in the sequence is also shown in Figure 8. It was also performed with n-hexadecane. However, in this experiment no water was included with the n-hexadecane that was fed to the anode of the fuel cell. As shown in (2), water reacts with the n-hexadecane in the anode half-cell reaction. The only water available for the sixth experiment would be the water in the phosphoric acid electrolyte. In principle the water removed from the phosphoric acid electrolyte at the anode could be replenished by water produced at the cathode, via its half-cell reaction. Equation (3) indicates that more water is produced by the cathode half-cell reaction than is consumed by the anode half-cell reaction (2).

The data in Figure 8 show that the fuel cell performance with n-hexadecane was slightly better when no water was fed to the anode. This suggests that n-hexadecane may compete with water for reaction sites in the anode catalyst layer. In any case the data in Figure 8 demonstrate that it is not necessary to feed water to the anode with the diesel fuel feedstock. In some respects fuel cell operation could be simpler if an anode water feeding system is not required. It also means that less water will have to be removed from the cathode.

Steady-state values for n-hexadecane were 0.42 V in Figure 5 and 0.39 V in Figure 8. Those n-hexadecane values can be compared with the values for canola biodiesel (0.4 V), soybean biodiesel (0.35 V), and petroleum diesel (0.38 V). There is not much difference among them, which is consistent with the H/C ratios obtained by ^{1}H NMR and ^{13}C NMR in Table 1.

Degradation was indicated by a decrease in potential during the initial portion of some of the time-on-stream experiments in Figures 5 and 8. The decrease of potential was attributed to degradation of the MEA. The condition of the MEA was documented by measuring hydrogen polarization curves at different times in the sequence of experiments.

The hydrogen polarization curves shown in Figure 9 were measured with hydrogen gas rather than diesel fuel when the MEA was in three different conditions. The middle curve (open circles) was measured after the first TOS experiment shown in Figure 5. Air at the cathode and hydrogen fuel at the anode of a phosphoric acid fuel cell normally produce an open circuit potential in the 0.8–0.9 volt range [22]. The open circuit potential for the middle curve, 0.82 V, is within the 0.8–0.9 volt range reported in the literature.

The hydrogen polarization curve measured at the conclusion of all of the experiments (solid circles in Figure 9) is worse than the polarization curve obtained after one hexadecane TOS experiment (the middle curve in Figure 9). The hydrogen polarization curve at the end of the TOS experiments (solid circles in Figure 9) and the diesel fuel polarization curve at the end of the TOS experiments (Figure 4) were similar. That similarity supports the suggestion that the hydrogen flowing through the MEA was not contacting

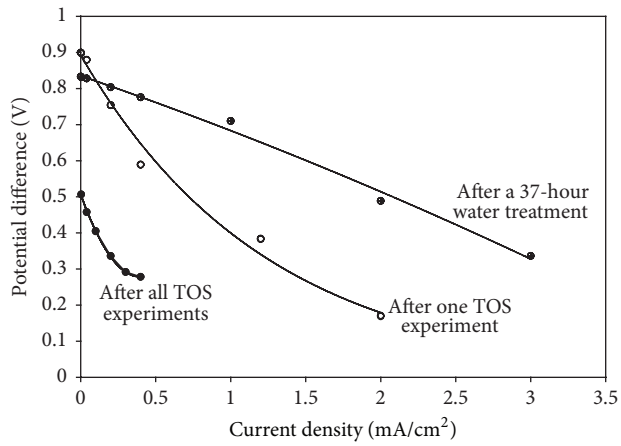

Figure 9: Polarization curve for a hydrogen fueled PAFC: potential difference (V) between the electrodes versus current density (mA/cm^2). Anode: hydrogen flow rate = 9.6 mL/min. Cathode: air flow rate = 245 mL/min. Temperature = 160°C. Pressure = 1 atm. Open circles are data points obtained after one TOS experiment with n-hexadecane. Solid circles are data points obtained after all TOS experiments with all diesel fuels. Open circles with "cross" signs are data points obtained after the degraded MEA had been regenerated during a 37-hour water treatment.

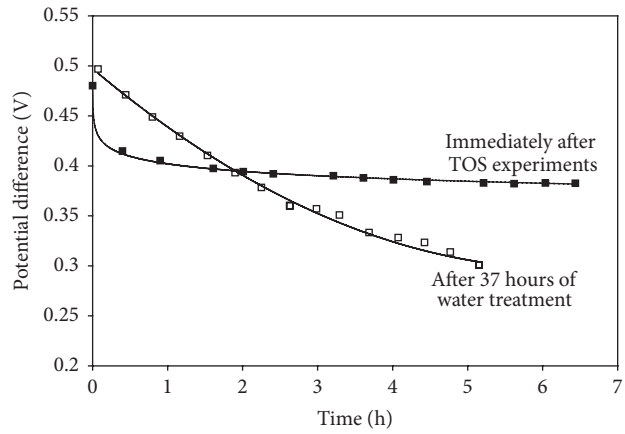

Figure 10: Polarization curves obtained with water as the only reactant flowing to the anode of a PAFC with an MEA that had been used for several TOS experiments with various diesel fuels: potential difference between the electrodes (V) versus time of water treatment (h). Anode: water flow rate = 5.1 mL/h. Cathode: air flow rate = 245 mL/min. Current density, j = 0.2 mA/cm^2. Temperature = 190°C. Pressure = 1 atm.

the catalyst surface and that the carbonaceous material that had accumulated on the MEA (not the hydrogen) was the material that was reacting at the anode. This observation is also consistent with the suggestion that the carbonaceous material is a reaction intermediate.

The upper polarization curve shown in Figure 9 (cross inside circles) was obtained after cleaning the MEA by flowing water through the anode after the MEA had been used in all the TOS experiments. The water at the anode could react with the accumulated carbonaceous deposits to form carbon dioxide, via an electrochemically assisted carbon-steam reaction. The improved polarization curve is consistent with water removing the carbonaceous deposits thereby making additional reaction sites available for the hydrogen reaction at the anode. The open circuit potential for the cleaned MEA in Figure 9 is less than that for the MEA that had been used in only one TOS experiment. The same phenomenon had been observed in Figure 2 and in the comparison between Figures 3 and 4. This observation is also consistent with the suggestion that the carbonaceous material is a reaction intermediate.

Experiments in Figure 10 were performed at a current density of 0.2 mA/cm^2 using water as the only reactant fed to the anode. The fuel for the reaction that created the current was attributed to a carbonaceous deposit on the MEA. The carbonaceous deposit would have been gradually consumed when the water reacted with the carbon, as the reaction continued. Two different situations are shown in Figure 10. The data shown as solid squares were obtained using the MEA immediately after the diesel fuel TOS experiments. Later that MEA was treated with water for 37 hours. Then a hydrogen polarization curve was measured. The data shown as open squares represent an additional 5 h of water treatment after the hydrogen polarization curve measurements. At time = 0 h, in Figure 10, the potential difference for both curves was near 0.5 V. The value of 0.5 V is also the value of the open circuit potential of one of the hydrogen polarization curves in Figure 9. That curve was measured in the presence of a hydrogen atmosphere reaction but the measurements were attributed to the reaction between carbonaceous material and water. On that basis the results in Figure 10 can also be attributed to the reaction of water with carbonaceous material even though water was the only reactant being fed to the fuel cell.

The experiment in Figure 10 performed after the 37-hour water treatment had a much greater rate of decrease in potential difference than the one performed immediately after the diesel fuel TOS experiments. However, the rates of reacting the carbonaceous material (current density = 0.2 mA/cm^2) were identical. That difference in rate of change of potential difference might be explained by the MEAs containing different amounts of carbonaceous material. When the change in amount of carbonaceous material on the anode surface is small compared to the total amount of carbonaceous material (MEA after TOS experiments), the fraction of the anode surface covered by carbonaceous material should be almost constant. In that case the potential difference, in Figure 10, is almost constant. In contrast, when the change in amount of carbonaceous material on the anode surface compared to the total amount of carbonaceous material is substantial (MEA after 37 h of water treatment), then the fraction of the anode surface covered by carbonaceous material should decrease. The change in fraction of anode surface covered by carbonaceous material may be responsible for the greater rate of decrease in potential difference observed for the MEA that had 37 h of water treatment.

Some preliminary characterization measurements of the MEAs were made by scanning electron microscopy, SEM, and

by energy dispersion spectroscopy, EDS. A SEM comparison of the fresh MEA with the used MEA showed that material had been deposited on the anode of the used MEA. EDS measurements on the used anode MEA indicated that carbon was the major element in the deposits. The presence of deposits on the anode, observed by SEM, and the identification of carbon in those deposits by EDS are consistent with the explanation that carbonaceous material may have been the cause of the degradation in fuel cell performance that was observed in this work.

As mentioned previously there was a difference in open circuit potential, OCP, between the cleaned MEAs and the used MEAs whose performance had degraded (Figures 2 and 9). The SEM measurements were consistent with carbonaceous material being deposited on the electrode microstructure. The data presented here definitely suggest that the carbonaceous deposits are associated with performance degradation. However, the observations also suggest that carbonaceous material is a reaction intermediate (Figures 5 and 8). At first it may seem that there is a conflict between carbonaceous material causing performance degradation while simultaneously being a reaction intermediate. A thermodynamic argument can be suggested to explain these two conflicting observations. As performance degradation occurs, eventually the concentration of carbonaceous material on the catalyst surface reaction sites becomes large enough, compared to the concentration of the reactant species in the fluid surrounding the catalyst, so that the driving force for the deposition of additional carbonaceous material diminishes. A steady state would be attained when the rate of deposition of carbonaceous material (caused by a diminished driving force) was equal to the rate at which the carbonaceous material (the reaction intermediate) was converted to products that leave the catalyst surface.

4. Summary

A 15-hour period of steady-state operation was demonstrated using petroleum diesel in a direct hydrocarbon phosphoric acid fuel cell. A relationship was found between the potential difference between the fuel cell electrodes at steady state and the H/C atomic ratio as determined by NMR measurements. A greater H/C ratio in the diesel fuel feedstock correlates with a greater potential difference between the fuel cell electrodes.

The degradation in fuel cell performance was attributed to the deposition of carbonaceous material on the anode catalyst of the MEA. Degradation was indicated by the difference in performance between cleaned and used MEAs, in Figures 2 and 3. There were several observations consistent with the suggestion that the carbonaceous material was a reaction intermediate. (a) The results in Figure 5 indicate that no net accumulation of carbonaceous material occurred at steady state. That might have occurred if at steady state the rate of deposition of carbonaceous material had been equal to its rate of removal (by reaction). (b) At open circuit potential the used MEA (containing a greater amount of carbonaceous material) had a smaller potential difference than the clean MEA (containing a lesser amount of carbonaceous material) (see Figure 2 and a comparison of the data in Figure 4). (c) The hydrogen polarization curve obtained using the MEA that had been used in all the TOS experiments in Figure 9 was similar to the diesel fuel polarization curves in Figures 3 and 4. (d) The polarization curves in Figure 10 obtained with water as the only feedstock showed that the rate of decrease in potential difference was much smaller when there was an abundance of carbonaceous material on the MEA. The presence of carbonaceous deposits on the MEA was indicated by the fact that electrical current and power were produced when water was the only reactant fed to the anode. After water treatment, the cleaned MEA would typically require more than 10 hours to redeposit a sufficient quantity of carbonaceous material to develop a steady-state reaction condition.

The electrochemical driving force for the fuel cells was correlated with the number of available aliphatic hydrogen atoms per carbon atom of feedstock molecule. It was found that water for the reaction at the anode could be provided by water in the phosphoric acid electrolyte. In principle, water in the electrolyte could be made-up by water produced at the cathode. That could simplify the fuel cell system by eliminating the need for a water feed system.

Conflict of Interests

The authors declare that there is no conflict of interests regarding the publication of this paper.

Acknowledgments

The authors gratefully acknowledge that this research and development project was supported by a grant from Transport Canada's Clean Rail Academic Grant Program and by a Discovery grant from the Canadian Government's Natural Sciences and Engineering Research Council. The material described in this paper is part of a thesis: Y. Zhu, M.A.Sc. Dissertation, "n-Hexadecane, Petroleum Diesel, and Biodiesel Fuels for a Direct Hydrocarbon Phosphoric Acid Fuel Cell," University of Ottawa, 2015.

References

[1] Z. F. Zhou, C. Gallo, M. B. Pague, H. Schobert, and S. N. Lvov, "Direct oxidation of jet fuels and Pennsylvania crude oil in a solid oxide fuel cell," *Journal of Power Sources*, vol. 133, no. 2, pp. 181–187, 2004.

[2] Y. Shiratori, T. Q. Tran, Y. Takahashi, and K. Sasaki, "Application of biofuels to solid oxide fuel cell," *ECS Transactions*, vol. 35, no. 1, pp. 2641–2651, 2011.

[3] T. Quang-Tuyen, Y. Shiratori, and K. Sasaki, "Feasibility of palm-biodiesel fuel for a direct internal reforming solid oxide fuel cell," *International Journal of Energy Research*, vol. 37, no. 6, pp. 609–616, 2013.

[4] H. Kim, S. Park, J. M. Vohs, and R. J. Gorte, "Direct oxidation of liquid fuels in a solid oxide fuel cell," *Journal of the Electrochemical Society*, vol. 148, no. 7, pp. A693–A695, 2001.

[5] Y. Zhu, T. Robinson, A. Al-Othman, A. Y. Tremblay, and M. Ternan, "n-hexadecane fuel for a phosphoric acid direct hydrocarbon fuel cell," *Journal of Fuels*, vol. 2015, Article ID 748679, 9 pages, 2015.

[6] H. Kishimoto, K. Yamaji, T. Horita et al., "Feasibility of liquid hydrocarbon fuels for SOFC with Ni-ScSZ anode," *Journal of Power Sources*, vol. 172, no. 1, pp. 67–71, 2007.

[7] D. Ding, Z. Liu, L. Li, and C. Xia, "An octane-fueled low temperature solid oxide fuel cell with Ru-free anodes," *Electrochemistry Communications*, vol. 10, no. 9, pp. 1295–1298, 2008.

[8] H. Liebhafsky and W. Grubb, "Normal alkanes at platinum anodes," *American Chemical Society, Division of Fuel Chemistry, Preprints*, vol. 11, 1967.

[9] E. J. Cairns, "Anodic oxidation of hydrocarbons and the hydrocarbon fuel cell," *Advances in Electrochemistry Science and Electrochemical Engineering*, vol. 8, pp. 337–392, 1971.

[10] J. O. M. Bockris and S. Srinivasan, "Electrochemical combustion of organic substances," in *Fuel Cells: Their electrochemistry*, pp. 357–411, McGraw-Hill, New York, NY, USA, 1969.

[11] H. A. Liebhafsky and E. J. Cairns, "The direct hydrocarbon fuel cell with aqueous electrolytes," in *Fuel Cells and Fuel Batteries*, pp. 458–523, Wiley, New York, NY, USA, 1968.

[12] S. Bertholet, *Oxydation electrocatalytique du methane [Ph.D. thesis]*, Université de Poitiers, Poitiers, France, 1998.

[13] C. K. Cheng, J. L. Luo, K. T. Chuang, and A. R. Sanger, "Propane fuel cells using phosphoric-acid-doped polybenzimidazole membranes," *Journal of Physical Chemistry B*, vol. 109, no. 26, pp. 13036–13042, 2005.

[14] O. Savadogo and F. J. Rodríguez Varela, "Low-temperature direct propane polymer electrolyte membranes fuel cell," *Journal of New Materials for Electrochemical Systems*, vol. 4, no. 2, pp. 93–97, 2001.

[15] F. J. Rodríguez Varela and O. Savadogo, "Real-time mass spectrometric analysis of the anode exhaust gases of a direct propane fuel cell," *Journal of the Electrochemical Society*, vol. 152, no. 9, pp. A1755–A1762, 2005.

[16] P. Heo, K. Ito, A. Tomita, and T. Hibino, "A proton-conducting fuel cell operating with hydrocarbon fuels," *Angewandte Chemie—International Edition*, vol. 47, no. 41, pp. 7841–7844, 2008.

[17] S. Srinivasan, *Fuel Cells: From Fundamentals to Applications*, Springer, New York, NY, USA, 2006.

[18] A. J. Appleby, "Fuel cells—phosphoric acid fuel cells: an overview," in *Encyclopedia of Electrochemical Power Sources*, J. Garche, Ed., pp. 533–547, Elsevier, Amsterdam, The Netherlands, 2009.

[19] A. Y. Tremblay and M. A. Dubé, "Fuel additive from plant oils, animal fats; for diesel engines," Article ID 8366794, US patent # 8366794 B2, 2013.

[20] C. G. Farrell, C. L. Gardner, and M. Ternan, "Experimental and modelling studies of CO poisoning in PEM fuel cells," *Journal of Power Sources*, vol. 171, no. 2, pp. 282–293, 2007.

[21] R. C. Zambiazi, R. Przymbylski, M. W. Zambiazi, and C. B. Menonca, "Fatty acid composition of vegetable oils and fats," *Boletim do Centro Pesquisa Processamento de Alimentos*, vol. 25, no. 1, pp. 111–120, 2007.

[22] R.-H. Song, C.-S. Kim, and D. R. Shin, "Effects of flow rate and starvation of reactant gases on the performance of phosphoric acid fuel cells," *Journal of Power Sources*, vol. 86, no. 1, pp. 289–293, 2000.